Enhanced SOGI Controller for Weak Grid Integrated Solar PV System

Firdous Ul Nazir, Nishant Kumar *Member, IEEE*, Bikash C. Pal, *Fellow, IEEE* Bhim Singh, *Fellow, IEEE,* and Bijaya K. Panigrahi *Senior Member, IEEE*

***Abstract*—This paper presents a two-stage three-phase solar photovoltaic (PV) system, which is controlled through a novel enhanced second order generalized integrator (ESOGI) based control technique. The proposed ESOGI is used for fundamental component extraction from nonlinear load current and distorted grid voltages. This integrator effectively and simultaneously manages to address the DC offset, inter-harmonic and integrator delay problems of the traditional SOGI. In addition, this control technique provides power factor correction, harmonic elimination, and load balancing functionalities. The ESOGI controller is used to generate reference grid currents for controlling the voltage source converter (VSC), interfacing the PV panel with the grid. Extensive simulation and experimental results on a developed prototype in the laboratory, depict that the total harmonic distortion (THD) of the grid injected currents and voltages are found well under IEEE-519 standard.**

***Index Terms*—Solar photovoltaic (PV) system, maximum power point tracking (MPPT), second order generalized integrator (SOGI), power quality.**

I. Introduction

THE decarbonisation and decentralisation of power generation have spurred the growth of renewables especially solar photovoltaics (PV). These PV systems are either used in a standalone mode with appropriate battery storage facilities or as a grid integrated system [2]-[4]. However, harnessing solar energy comes with its own challenges, most important of them are discussed in [1]. The PV technology is an effective way to harness the solar energy for electricity production. The requirement of storage batteries puts the stand alone PV systems at an economical disadvantage against the grid integrated PV systems. Thus, the grid integrated systems are more prevalent especially where the grid is available [5]-[7].

The rapid proliferation of non-linear loads due to power electronic switching used in magnetic ballast, and light emitting diodes is adversely affecting the power quality of the utility grid. These loads inject harmonic currents into the grid. This situation is particularly challenging for the PV integration and the requirement of injecting balanced positive sequence currents into the grid needs the extraction of fundamental positive sequence component from the polluted load current. Several different types of control schemes have been proposed in the literature to meet this requirement. The noteworthy of these PV integration control schemes are synchronous frame theory [8], enhanced phase locked loop [9], instantaneous reactive power theory [10], extended observer based sliding mode control technique [11], fuzzy-logic based control [12], fourth order generalized filter [13], adaptive notch filter [14], and an adaptive control scheme [15].

The most commonly employed control technique for the control of the interfacing inverter for the grid tied PV system is the second order generalized integrator (SOGI); because of its robustness and ease of implementation [16]. The SOGI acts as a building block for the orthogonal signal generator (OSG) and hence can be either used directly for frequency estimation as a frequency locked loop [17] or indirectly through the dq frame mapping [18]. The traditional SOGI controller, however, suffers from three major disadvantages - a) the estimation is erroneous if the input signal has a DC offset, b) ripple content or inter-harmonics in the input signal also lead to wrong estimation, and c) the usage of integrators in the control structure introduces the integrator delay in the estimation process. Various solutions have been proposed in the literature to deal with these problems. Ghartemani *et al.* [19] addressed the DC component problem of the SOGI algorithm by introducing a new loop inside the SOGI structure. This additional loop adds another integrator to the SOGI controller and helps in the estimation of the DC offset in the input; the estimated DC value is directed towards the output for its complete cancellation in the final signal. Similarly, Golestan *et al.* [20] addressed this DC component challenge by proposing a novel phase locked loop (PLL) structure known as DC Immune-PLL (DCI-PLL). They have been able to successfully achieve the DC component rejection by comparing the current and the delayed value of the signal under consideration. Further, Matas *et al.* [21] have proposed a cascaded double SOGI approach for the DC-offset voltage distortion problem of the conventional SOGI. Infact this cascaded double SOGI structure is sensitive to all kinds of subharmonics present in the signal and could effectively remove all of these simultaneously. The ripples or the inter-harmonics are effectively filtered by the damped-SOGI algorithm proposed in [22]. The damped-SOGI implementation adds a feedback loop across the forward path integrator; this feedback loop introduces a damping term on the basic SOGI control, hence filtering out the ripples in the input signal. Finally, the integrator delay problem is overcome by discretizing the SOGI controller [23]. Since these

F. Ul Nazir and B. C. Pal are with the Electrical and Electronic Engineering Department, Imperial College, London SW7 2AZ, U.K. (e-mail: f.ul-nazir16@imperial.ac.uk; b.pal@imperial.ac.uk).

N. Kumar is with the Electrical and Computer Engineering Department, National University of Singapore, 119077, Singapore (email: nishant.kumat1729@gmail.com).

B. Singh and B. K. Panigrahi are with the Department of Electrical Engineering, Indian Institute of Technology Delhi, New Delhi, 110016, India (email: bhimsing156@gmail.com; bkpanigrahi@ee.iitd.ac.in).

This work is supported by the JUICE project under Contract EP/P003605/1 and Indo-UK project UKCERI.

challenges are not usually system specific and can occur in the same system simultaneously or at different time intervals, thus there is a need for an improved and robust SOGI controller which is equipped with all the three functionalities. This is the main aim of this paper to present such an ESOGI control scheme.

The rest of the paper is organised as follows: Section II discusses the system configuration with the help of a representative figure. Section III presents the main control aspects of the two stage grid tied PV system. The full control scheme includes an MPPT controller and the proposed ESOGI for efficient grid synchronisation of the PV system. The elaborate experimental results with appropriate discussions are presented in Section IV. The proposed controller is tested under various conditions of load imbalance, harmonics, and varying solar insolation. Finally, the paper is concluded in Section V.

II. System Configuration

The system configuration is shown in Fig. 1. The full system comprises of a PV string, which is a combination of small PV panels connected in series and parallel, a boost or step up converter, a DC link capacitor, a 3-phase insulated gate bipolar transistor (IGBT) based VSC, interfacing inductors, ripple filter, linear and non-linear loads and a three phase grid. The appropriate control of the VSC and the grid synchronization is achieved aptly by the proposed controller, while a maximum power point tracking (MPPT) controller is used to control the boost controller in order to extract maximum power from the PV panel. Since both the grid and the AC side of the VSC behave as voltage sources, so they are connected through series inductors, which absorb the instantaneous voltage differences between them. Moreover, interfacing inductors help in smoothening the output current of the VSC. Therefore, the selection of their inductance values depend on the allowable current ripple. The voltage at the point of common coupling (PCC) is filtered for any ripple harmonics by connecting a ripple filter in shunt at the PCC. These ripples are generated by the switching of the VSC. A combination of linear and non-linear local loads are also fed from the PCC. The non-linear load is emulated by connecting an RL load bank through diode bridge rectifier. The ratings of the components for the laboratory prototype are decided by the various key relations given in [24].

III. Control Philosophy

A two stage control is employed to not only effectively generate appropriate gating pulses for the VSC but also to operate the PV system at its maximum power point. The maximum power point tracking (MPPT) of the PV system is achieved by the perturb and observe (P&O) algorithm. The P&O algorithm is the most widely used MPPT scheme due to its simplicity and ease of implementation [25]-[26]. The MPPT algorithm generates the reference DC link voltage corresponding to the maximum power point at the current operating conditions.

A. Control Algorithm for the VSC Switching

The full control scheme for generating the VSC gating pulses is depicted in Fig. 2. The full control scheme is subdivided into certain sections such as generation of unit templates, extraction of fundamental component of the load current, estimation of the loss term, calculation of the PV feed-forward term, and generation of the 3-phase reference grid currents. The reference grid currents are utilized to generate switching pulses for the VSC switches.

1) Generation of Unit Templates: The unit templates are computed by sensing only two line voltages whose fundamental components are extracted by using the ESOGI - which effectively filters out any harmonics present in the sensed signals. The filtered line voltages are then used to estimate the 3-phase voltages through the following transformation.

$$\begin{bmatrix} V_{ga} \\ V_{gb} \\ V_{gc} \end{bmatrix} = 1/3 \begin{bmatrix} 2 & 1 \\ -1 & 1 \\ -1 & -2 \end{bmatrix} \begin{bmatrix} V_{gab} \\ V_{gbc} \end{bmatrix} \tag{1}$$

The computed 3-phase voltages are used for calculating the terminal voltage (V_t) at the PCC, which is defined as follows [27],

$$V_t = \sqrt{\frac{2}{3}(V_{ga}^2 + V_{gb}^2 + V_{gc}^2)} \tag{2}$$

The in-phase (u_{pa}, u_{pb} and u_{pc}) and quadrature-phase (u_{qa}, u_{qb} and u_{qc}) unit voltage templates are estimated using the positive sequence 3-phase grid voltage and the magnitude of the terminal voltage at the PCC, as follows,

$$\begin{bmatrix} u_{pa} \\ u_{pb} \\ u_{pc} \\ u_{qa} \\ u_{qb} \\ u_{qc} \end{bmatrix} = \frac{-1}{2\sqrt{3}V_t} \begin{bmatrix} -2\sqrt{3} & 0 & 0 \\ 0 & -2\sqrt{3} & 0 \\ 0 & 0 & -2\sqrt{3} \\ 0 & 2 & -2 \\ 3 & -1 & 1 \\ -3 & -1 & 1 \end{bmatrix} \begin{bmatrix} V_{ga} \\ V_{gb} \\ V_{gc} \end{bmatrix} \tag{3}$$

2) Extracting Fundamental Component of the Load Current: The structure of the proposed ESOGI is shown in Fig. 3. The ESOGI extracts the fundamental positive sequence component (K_i') and a orthogonal component (K_i'') of the input signal (i_l). The ESOGI filter makes use of three discrete integrators. ESOGI is the enhanced version of the classical SOGI. In the first step, SOGI is discretized by using a trapezoidal concept of the integrator, which is more accurate with respect to forward or backward Euler discrete integrator. The discrete SOGI is described as,

$$\int \rightarrow \frac{\xi T_s(z+1)}{(z-1)} \tag{4}$$

The accuracy of the discrete integrator is further enhanced by using noise eliminating factor, which is described as,

$$\int \rightarrow \frac{\xi T_s(z+e^{-\sigma T_s})}{(z-e^{-\sigma T_s})} \tag{5}$$

Where T_s is the sampling time, ξ is integrator gain, and σ is the noise eliminating constant.

The issue of DC offset is solved by using a separate feedback loop, which extracts the DC component from the output signal and subtracts it from the input signal. Therefore

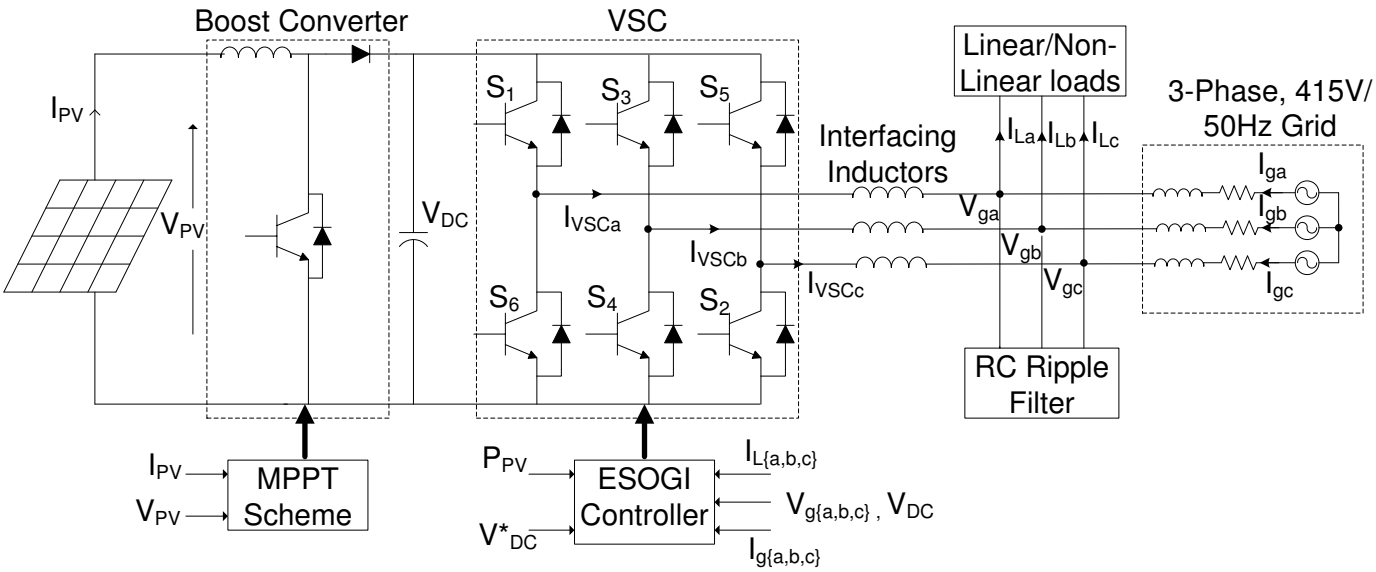

Fig. 1: System Configuration

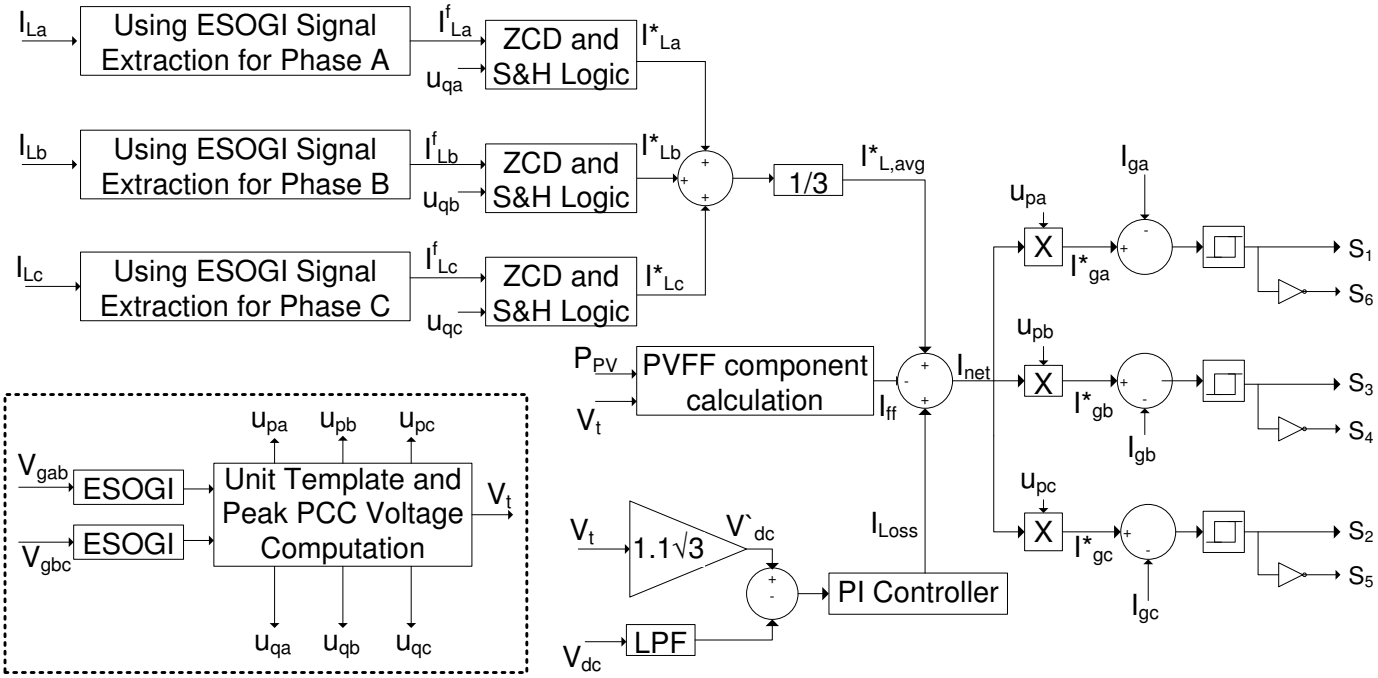

Fig. 2: Structure of control algorithm for switching of VSC

the ESOGI is capable to eliminate the DC offset, noise and delay from the input signal.

The open loop transfer functions for the extracted in-phase k_i' and quadrature-phase k_i'' components of the input signal, i_l are given as,

$$\frac{k_i'}{i_l} = \frac{5K\beta + K\beta^2}{5 + 10K\beta + (5+K)\beta^2 + 5K\beta^3} \tag{6}$$

$$\frac{k_i''}{i_l} = \frac{1}{5(1+K\beta)} \times \left[\frac{k_i'}{i_l}\left\{(5+K)\beta + 5K\beta^2\right\} - K\beta\right] \tag{7}$$

where β is given as,

$$\beta = \frac{\omega\xi T_s(z + e^{-\sigma T_s})}{(z - e^{-\sigma T_s})} \tag{8}$$

Fig. 4 compares the performance of the ESOGI and the conventional SOGI through their Bode diagrams for both the in-phase and orthogonal transfer functions. The Bode plots of both these transfer functions clearly depict better performance of the ESOGI controller over that of the conventional SOGI in terms of the filtering capability. This is because the magnitude plot in both the transfer functions has a relatively lower value in the lower frequency spectrum for the ESOGI controller which shows better harmonic and interharmonic mitigation

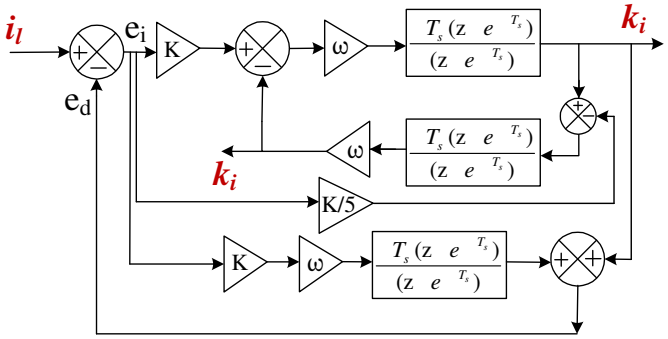

Fig. 3: Structure of the ESOGI

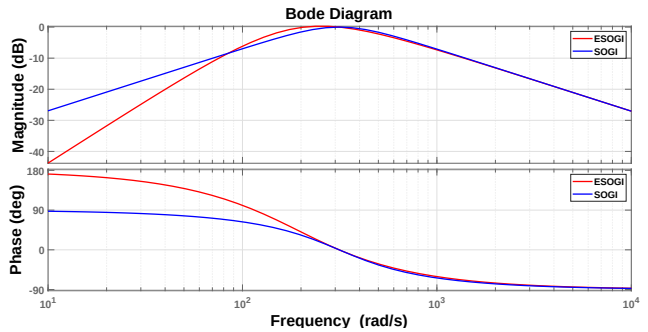

(a)

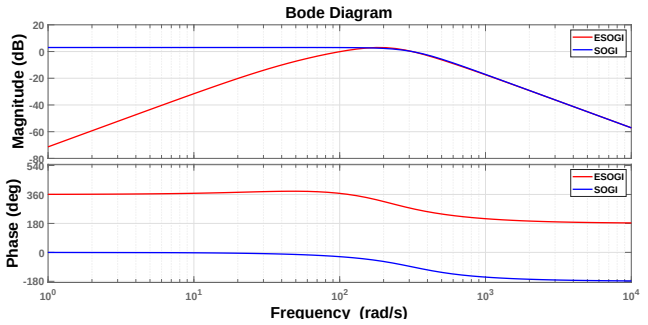

(b)

Fig. 4: (a) Bode plot for in-phase component transfer function (b) Bode plot for quadrature-phase component transfer function

capabilities. In addition to this, Fig. 4b shows that the magnitude plot of the quadrature-phase component transfer function exhibits a positive gain in the lower frequency range for the traditional SOGI controller depicting that this controller is unable to eliminate the DC offset in the input signal. However, the same plot for the ESOGI controller is considerably below zero and hence ESOGI possesses good DC offset impact mitigation property.

3) Parameter Design Procedure: The tuning of the parameters for the ESOGI is done in the 's' domain. The open loop transfer function for the in-phase component in the 's' domain is written as:

$$\frac{k_i'}{i_l} = G_{ip}(s) = \frac{5K\omega s^2 + K\omega^2 s}{5s^3 + 10K\omega s^2 + (5+K)\omega^2 s + 5K\omega^3} \quad (9)$$

The characteristic equation of the controller is easily derived from (9) as follows:

$$1 + G_{ip}(s) = 0 \quad (10)$$

$$s^3 + 3K\omega s^2 + (1 + 0.4K)s + K\omega^3 = 0 \quad (11)$$

The stability of (11) is analysed through the Routh's stability criteria. During this stability analysis procedure the quantities in the first column are always maintained positive. The most suitable value of the parameter K is found to be:

$$K = 0.5 \quad (12)$$

It is evident that the parameter tuning process is simple as compared to other related techniques in the literature. This is because of the unique property of the proposed controller that it needs tuning for only a single parameter (K) to determine the overall performance. While at the same time other related techniques proposed in the literature require tuning of more than one parameters. As an example the FLL-DR (frequecny locked loop with enhanced DC offset rejection) [19], and SOSF (second-order sequence filter) [28] have two tunable parameters. Moreover, the FOGI (fifth-order generalized integrator) [29] has three parameters and the $\alpha\beta$DSC (delayed signal cancellation) operator [30] even has five parameters which need to be tuned.

4) Estimation of the Loss Term: The loss component represents the required amount of power for maintaining the reference DC link voltage. This loss component is estimated by passing the error of the sensed DC link voltage (V_{dc}) and the reference DC link voltage (V_{dc}') through a PI controller. The adaptive reference DC link voltage is used, which is generated from the instantaneous value of the terminal voltage , V_t,

$$V_{dc}' = 1.1\sqrt{3}V_t \quad (13)$$

Moreover, the sensed DC link voltage is filtered through a low pass filter (LPF) before its comparison with the reference DC link voltage. This means the loss term is estimated as follows:

$$I_{Loss} = (k_p + k_i/s)(V_{dc}' - V_{dc}) \quad (14)$$

5) Computation of PV Feed-Forward Component: For a fast dynamic response, towards the changes in solar insolation and the terminal grid voltage, a term known as PV feed-forward (PVFF) component is used in the control scheme. When the solar insolation changes, the net active power fed into the grid also changes, which manifests through oscillations in the grid currents - which are mitigated by the PVFF component. This component is computed as,

$$I_{ff} = \frac{2P_{PV}}{3V_t} \quad (15)$$

It is clear from (15) that the instantaneous changes in the solar insolation and grid voltage are reflected in the PVFF component through P_{PV} and V_t respectively. It is also clear that PVFF component is present in the control only when the system is working in the grid integrated mode. However, when the solar insolation falls to zero and the PV system begins to render ancillary services in the D-STATCOM mode the PVFF term vanishes as the generated PV power, P_{PV}, becomes zero.

6) Computation of Net Grid Current Component: The grid currents are assumed to come out of the grid terminals and since the losses and the local load currents are assumed to be drawn from the grid while as the PVFF component is fed into the grid, the net grid current component is computed as follows,

$$I_{net} = I^*_{L,avg} + I_{Loss} - I_{ff} \tag{16}$$

Here, $I^*_{L,avg}$ is the average per phase active component of load currents. The load current of each phase is filtered for the harmonic distortions to obtain the corresponding fundamental components by passing each of them separately through the proposed ESOGI controller. These sinusoidal fundamental components are given as an input to a sample and hold (S&H) logic which is triggered by a zero crossing detector (ZCD) logic; the ZCD is inturn triggered by the quadrature-phase unit template corresponding to the same phase. This procedure extracts a constant active component I^*_{Labc} of the phase load currents. Thus, the average per phase active component of load currents is given as,

$$I^*_{L,avg} = \frac{I^*_{La} + I^*_{Lb} + I^*_{Lc}}{3} \tag{17}$$

7) Generation of VSC Switching Pulses: The 3-phase reference grid currents (I'_{ga}, I'_{gb}, and I'_{gc}) are computed by multiplying the respective in-phase unit voltage templates with the net load component of the current.

$$I'_{ga} = I_{net} u_{pa} \tag{18}$$

$$I'_{gb} = I_{net} u_{pb} \tag{19}$$

$$I'_{gc} = I_{net} u_{pc} \tag{20}$$

The comparison of these reference grid currents with the sensed grid currents (I_{ga}, I_{gb}, and I_{gc}) produces the error, which is processed by the indirect hysteresis current controller to generate switching pulses for the appropriate switching of the VSC.

IV. Experimental Results

A prototype, shown in Fig. 5, for a two stage three phase PV grid integrated system is developed in the laboratory to verify the proposed controller. The PV power generating system is realized by a solar PV array simulator (AMETEK make ETS600 x 17DPVF) of 3.8 kW capacity with the maximum power point coordinates on the VI curve as (250 V, 15.2 A). The two line PCC voltages and the DC link voltage are sensed through Hall-Effect voltage sensors (LV25-P), while the three load currents along with the PV current are sensed by Hall-Effect type current sensors (LA55-P). The proposed controller is implemented on a digital signal processor (DSP, dSPACE-1104), while the electrical isolation between the high power VSC signals and the low power DSP signals is achieved by employing opto couplers. Various waveforms are recorded by a power analyzer (Fluke make, model: 43B) and a digital scope oscilloscope (Agilent make, model: DCO0614A). The list of parameters and other relevant quantities of the experimental set-up are given in Appendix.

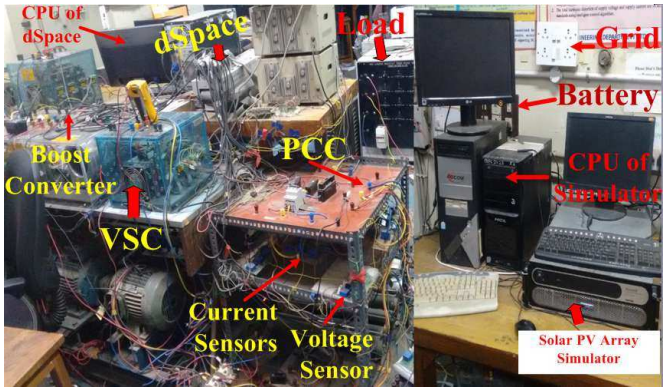

Fig. 5: Laboratory prototype of two stage three phase grid integrated system

A. Steady State Performance of the System Under Non-Linear Load

Fig. 6 depicts the steady state performance of the developed laboratory prototype when a non-linear local load is present at the PCC. Fig. 6a and Fig. 6b respectively show the voltage-current waveform of the phase 'a' of the grid and the active-reactive power injected into the grid. Similar waveforms for the VSC and the load are shown in Fig. 6c-6d and 6e-6f respectively. The negative sign of the grid active power in Fig. 6b implies that the grid absorbs active power which is supplied by the PV array. The load real power is also supplied by the PV array and hence the active power output from the VSC, as shown in Fig. 6d, is almost equal to the sum of the grid and load active powers. The slight discrepancy is owing to the various losses. It is also clear from these figures that the displacement power factor is unity for the grid, load and the VSC. The results of harmonic analysis of the various important signals are shown in the Fig. 6g-6j. The total harmonic distortion (THD) for the 'a' phase current of the VSC is reported as 10.2%; this higher value of the THD is due to the fact that the VSC supplies currents to the non-linear local load as well. The THD of the non-linear local load is way higher at 26.5% as is clear from Fig. 6h. However, it is clear from Fig. 6i and Fig. 6j that the THD of the grid current and the grid voltage is found to be well under the 5% specified in the IEEE-519 standard.

B. Dynamic Performance of the System Under Load Unbalance

Fig. 7 shows the dynamic performance of the grid integrated PV system when the 'a' phase load is withdrawn during the experiment. Fig. 7a shows that the phase 'a' grid current still remains sinusoidal even after the removal of that particular phase load, however the magnitude of the grid current increases after the load withdrawal so as to divert the lost phase 'a' load power to the grid. The dynamics in the phase 'b' are shown in Fig. 7b - it is clear that the grid current in this phase also exhibits the same behaviour as that of the phase 'a' i.e. remaining sinusoidal throughout and increasing in magnitude after the load unbalance. Various intermediate

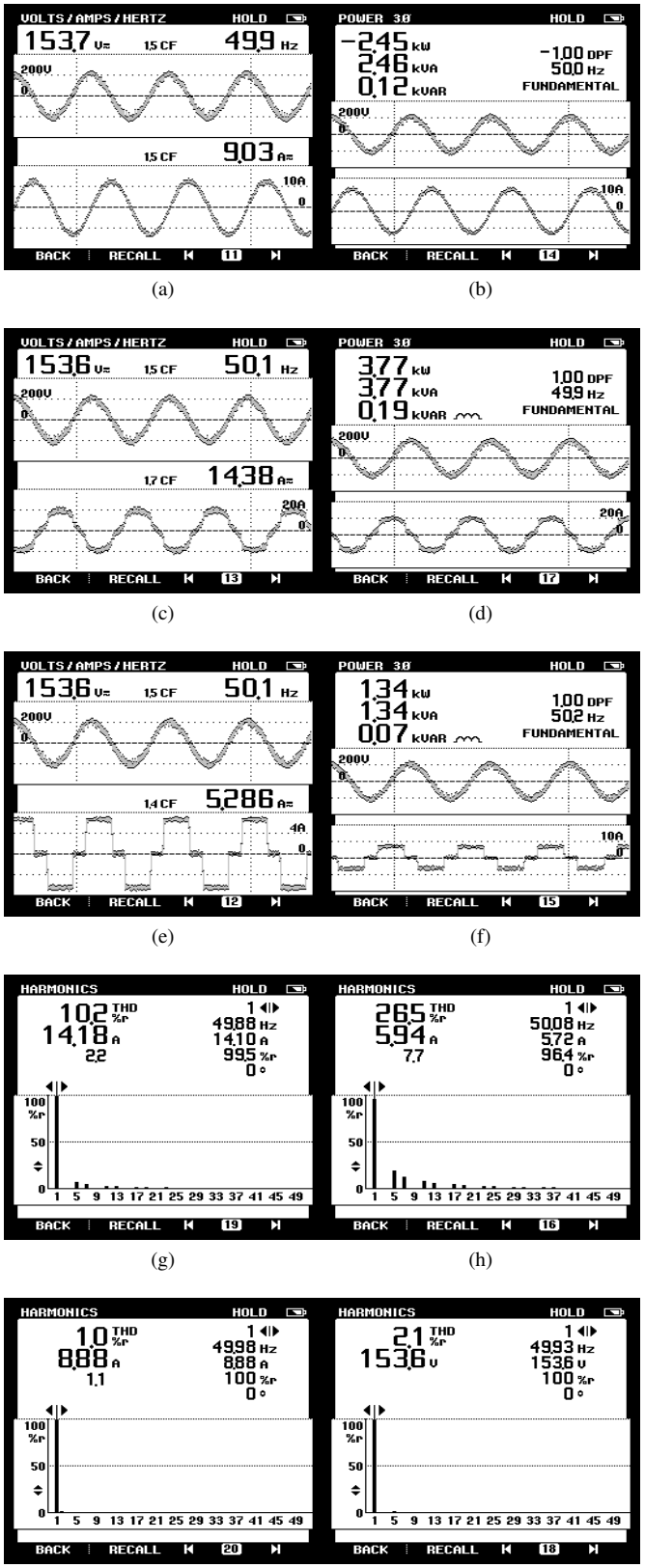

(a) (b) (c) (d) (e) (f) (g) (h) (i) (j)

Fig. 6: Steady state performace for non linear load (a) V_{gab}, I_{ga} (b) P_g, Q_g (c) V_{gab}, I_{vsca} (d) P_{vsc}, Q_{vsc} (e) V_{gab}, I_{La} (f) P_L, Q_L, THD of (g) I_{vsca} (h) I_{La} (i) I_{ga} (j) V_{gab}

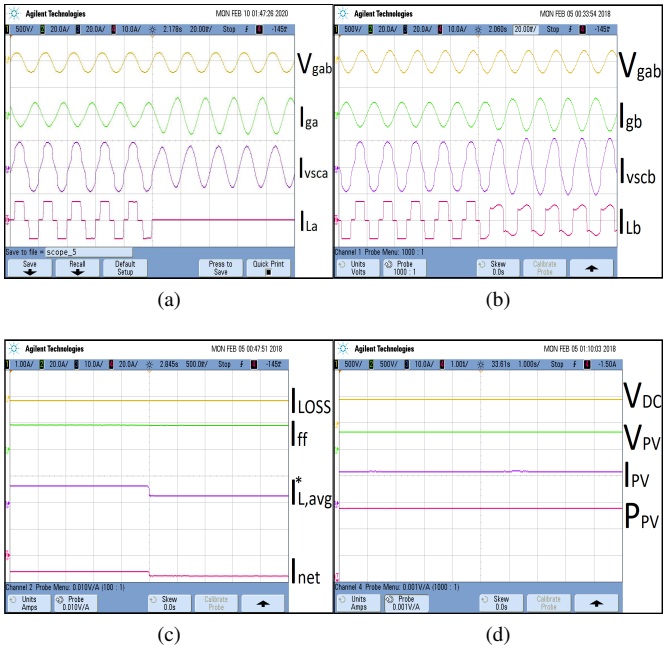

(a) (b) (c) (d)

Fig. 7: Dynamic response for Unbalanced non-linear load (a) $V_{gab}, I_{ga}, I_{vsca}, I_{La}$ (b) $V_{gab}, I_{gb}, I_{vscb}, I_{Lb}$ (c) $I_{LOSS}, I_{ff}, I^*_{L,avg}, I_{net}$ (d) $V_{DC}, V_{PV}, I_{PV}, P_{PV}$

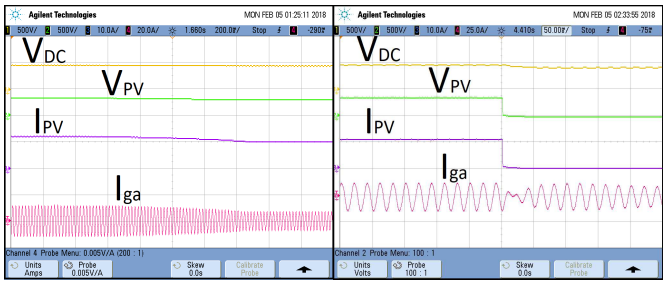

(a) (b)

Fig. 8: (a) Performance of the system under variable solar insolation (b) Behaviour of the system as a D-STATCOM

control signals are shown in Fig. 7c. It is clear that the loss component and the feed-forward component of the current remain unaltered. However, the removal of phase 'a' load manifests in a decrease of the average load current which in turn results in a corresponding net decrease in the net current signal of the controller. Finally, Fig. 7d demonstrates that various electrical signals like the DC link voltage, and PV voltage, current and power are not affected by the load removal, as is expected, because there is no change in the solar insolation.

C. Change in Solar Insolation

Fig. 8 depicts the behaviour of the system when the solar insolation changes. The first test under this category is carried by decreasing the solar insolation from 1000 W/m^2 to 800 W/m^2 and various signals of interest are shown in Fig. 8a. The DC link voltage is found to be stable whereas the PV

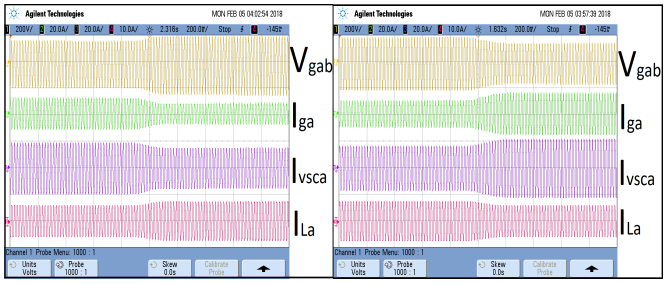

(a) (b)

Fig. 9: Performance of the system for (a) over voltage (b) under voltage

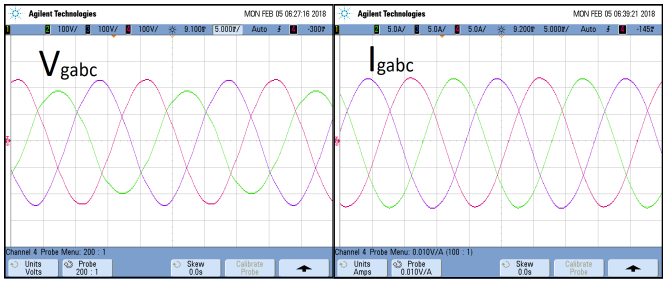

(a) (b)

Fig. 10: Dynamics of the controller for imbalanced grid voltages (a) $V_{gab}, V_{gbc}, V_{gca}$ (b) I_{ga}, I_{gb}, I_{gc}

voltage and current exhibit a decrement as the solar insolation is decreased, which is expected. The reduced solar insolation implies that the available PV output power also decreases and hence the power injected into the grid reduces, since the load is kept constant; this is evident as the phase 'a' grid current decreases in magnitude. The second test for this category is carried by abruptly removing the solar insolation and the performance in this case is displayed in Fig. 8b. The DC link voltage is maintained fairly stable by the PI controller. The output voltage and the current of the PV array collapse immediately due to lack of any solar insolation. Prior to removing the solar insolation, the PV array has been generating active power which is partly used to supply the load and partly being injected into the grid. However after the solar insolation collapses, the load is fed by the grid. This is clear from the phase 'a' grid current which changes its direction as the solar insolation goes to zero.

D. Performance for Under Voltage and Over Voltage Condition

The behaviour of the controller under the over and under voltage conditions is depicted in Fig. 9. The dynamics of various signals of interest for the over voltage case are shown in Fig. 9a. Since the loads connected at the PCC are constant impedance type, thus as the over voltage condition occurs the load current increases, and a greater share of PV generated power is taken by the load. This leaves the grid with a smaller uptake of the power. Hence, the grid current sag after the over voltage phenomenon is explained. However, it is evident that the grid currents remain balanced and sinusoidal all the time. Similarly, Fig. 9b shows the operation of the system for the under voltage situation. As expected, for the same reasons, the load current shows a dip whereas the grid current experiences a rise, but more importantly, remaining sinusoidal and balanced.

E. Behaviour of Controller for Imbalanced Grid Voltages

Fig. 10 depicts the behaviour of the controller for the scenario when the grid voltages are imbalanced. The imbalanced grid voltages are shown in Fig. 10a whereas the grid currents stay balanced as is evident from Fig. 10b. This is due to the fact that the positive sequence of the grid voltages are used for the computation of the unit templates. This procedure nullifies the imbalance, and a balanced set of reference grid currents is generated.

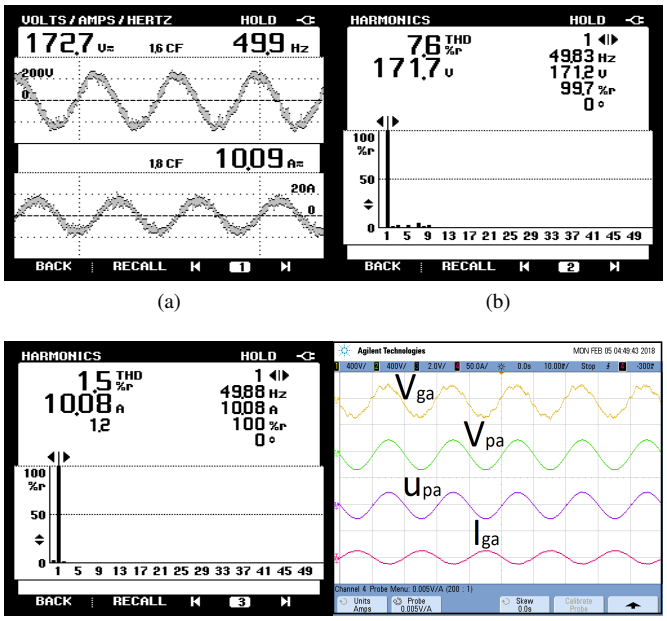

(a) (b)

(c) (d)

Fig. 11: Performance of the controller under distorted grid voltages

F. Performance of the Controller in Case of Distorted Grid Voltages

Fig. 11 shows the performance of the system for the scenario when the grid voltages are appreciably distorted. The waveform of the distorted grid voltage and the associated current is captured in Fig. 11a, while as the harmonic spectrum of the grid voltage is depicted in Fig. 11b, which clearly shows that the THD of the grid voltage is higher than the recommended level as per the IEEE 519 standard. The effectiveness of the controller is evident from Fig. 11c which shows the THD of the grid current. The THD is found to be just 1.5% which is well below the recommended upper limit of 5% as per the IEEE 519 standard. This means that the controller is able to maintain a distortionless sinusoidal grid current even when the grid voltage is distorted. Various internal signals

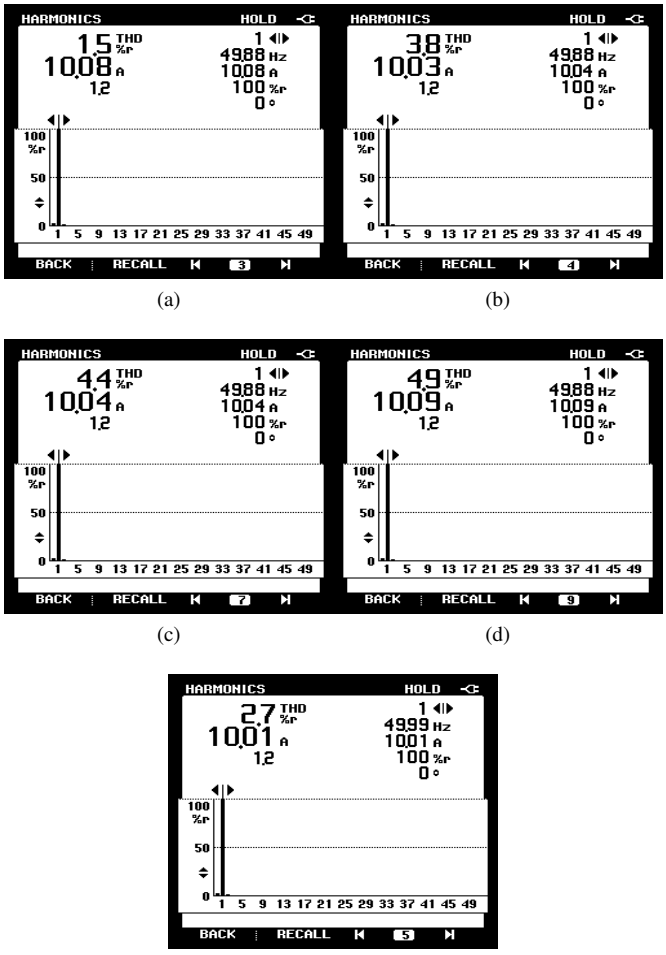

Fig. 12: THD analysis of the grid current in a distorted grid voltage scenario obtained through (a) ESOGI (b) DSOGI-GE (c) DCI-PLL (d) SOGI (e) MSOGI

of interest, which depict the functioning of the ESOGI, are shown in Fig. 11d. This figure shows that the unit templates and the positive sequence phase voltages are smooth and sinusoidal. This is because of the fact that the proposed controller uses the positive sequence phase voltages, rather than the actual voltages which are distorted in this case, to derive the unit templates. These smooth unit templates ensure the reference grid currents are distortionless with a permissible THD content.

1) Comparative Analysis: Fig. 12 shows the comparison of the ESOGI with different state of the art controllers available in the literature. The different controllers selected for the comparative analysis with the proposed ESOGI are Double Second-Order Generalized Integrator - Gradient Estimator (DSOGI-GE) [21], DC-Immune - Phase-Locked Loops (DCI-PLL) [20], SOGI [31], and Modified SOGI (MSOGI) proposed by Karimi *et al* [19]. The comparative tests are performed for a distorted grid voltage scenario with the same levels of distortion as given in Fig. 11b. All the controllers are able to achieve the grid current with a relatively lower distortion than the grid voltage. However, the main advantage of the ESOGI

TABLE I: Comparative analysis of grid current THD values achieved by state-of-the-art algorithms in comparison with the proposed algorithm

Operating Condition	Value of Grid Current THD for Different Algorithms			
	Proposed algorithm	MSOGI	DSOGI-GE	DCI-PLL
Normal operation with nonlinear loads (THD_{iL})	1.0%	2.5%	4.9%	3.6%
Low solar irradiation (100W/m^2)	4.6%	>5%	>5%	>5%
Grid under-voltage condition	1.5%	3.9%	3.4%	4.1%
Grid over-voltage condition	2.1%	4.2%	4.0%	4.7%
Imbalanced grid voltage condition	1.9%	3.7%	3.9%	5.5%
Distorted grid voltage condition	1.5%	2.7%	3.8%	4.4%
Night time operation (DSTATCOM mode)	1.7%	4.6%	3.4%	4.4%

TABLE II: Comparative performance analysis of state-of-the-art algorithms in comparison with the proposed algorithm

Parameters	Proposed algorithm	MSOGI	DSOGI-GE	DCI-PLL
Computational complexity	Low	Low	Medium	High
DC link voltage oscillations	Low	High	High	Medium
Accuracy	High	Low	medium	Poor
THD of grid current	Low	Poor	Medium	Medium
DSP speed	High	High	Low	High
Sampling time	30μs	30μs	40μs	30μs
Algorithm complexity	Medium	Low	Low	High
Requirement of cache memory	Low	Low	Low	High

is evident from the fact that it is able to achieve the lowest THD, of 1.5%, in the grid current among all of the controllers. The other controllers have a THD of more than 1.8 times the ESOGI in the grid current, with 3.8%, 4.4%, 4.9%, and 2.7% respectively for DSOGI-DE, DCI-PLL, SOGI, and MSOGI.

The comparative performance analysis of the proposed ESOGI against the state-of-the-art algorithms is also presented in Table I and II for detailed analysis. The conventional algorithms selected for this comparison are the MSOGI, DSOGI-GE and DCI-PLL. It is clear from Table I that the proposed control scheme performs better under all the operating conditions when the achieved THD values are compared. Moreover, Table II depicts the other advantages of the ESOGI like low computational burden, more stable DC link voltage, and control accuracy.

G. Solar PV to DSTATCOM Mode of Operation

Fig. 13 shows the response of the system when there is a loss of solar insolation. In such case, the solar PV system behaves as a DSTATCOM and continues to meet the reactive power requirements of the load connected at the PCC. It is clear from Fig. 13a that as the DSTATCOM mode sets in, the grid current undergoes a 180^o phase reversal - which implies that the load active power is now being supplied by the grid

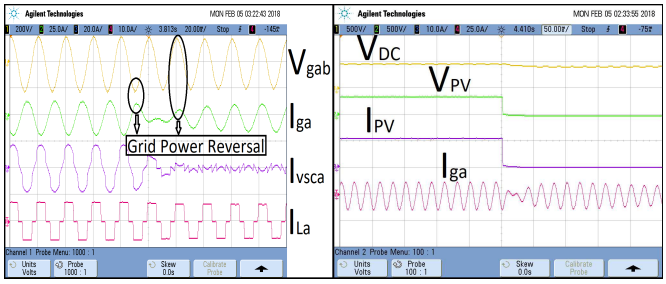

(a) (b)

Fig. 13: Transition from PV to DSTATCOM mode (a) $V_{gab}, I_{ga}, I_{vsca}$ (b) $V_{DC}, V_{PV}, I_{PV}, I_{ga}$

in the absence of the PV power. Fig. 13b shows that the PV current, and consequently the PV power, is reduced to zero in the DSTATCOM mode. However, the controller is able to maintain a stable DC link voltage irrespective of the transition.

V. Conclusion

A novel enhanced second order generalized integrator (ES-OGI) based control technique has been proposed for the integration of two stage three phase PV system with the grid. The proposed controller has been found to exhibit better performance in respect to most of the conventional second order generalized integrator (SOGI) based controls in terms of fast convergence rate, good noise immunity, DC offset removal, and ripple harmonics damping. The proposed controller has been found to produce good steady state and dynamic performance under the influence of unbalanced non linear loads, distorted voltages, and varying solar insolation conditions. In case the solar insolation is absent, at night or during clouds, the system operates as a D-STATCOM and continues to provide the ancillary services for effective mitigation of PQ issues. Under all the operating conditions, the THD of the grid current is found to be well under the threshold set in the IEEE 519 standard. Extensive simulation and experimental tests imply the proposed controller is feasible for the grid integrated PV systems.

Appendix

Simulation parameters: Three phase grid voltage = 150 V, system frequency = 50 Hz, supply inductance = 200 mH, supply resistance = 150 Ω, interfacing inductor = 3.5 mH, ripple filter resistance = 3 Ω, ripple filter capacitance = 3.7 μF, K_p = 0.1, K_i = 0.001, PV array open circuit voltage = 290.4 V, PV array short circuit current = 15.68 A, PV peak power = 3.8 kW.

Experimental parameters: Three phase grid voltage = 150 V, system frequency = 50 Hz, interfacing inductance = 4 mH, ripple filter resistance = 5 Ω, ripple filter capacitance = 5 μF, K_p = 0.23, K_i = 0.001, PV open circuit voltage = 290.4 V, PV short circuit current = 15.68 A, PV peak power = 3.8 kW.

References

[1] Y. Li, S.S. Choi, C. Yang, and F. Wei, "Design of variable-speed dish-stirling solar-thermal power plant for maximum energy harness," *IEEE Trans. Energy Convers.*, vol. 30, no. 1, pp. 394-403, Mar. 2015.

[2] X. B. Kjaer, J. K . Pedersen, and F. Blaabjerg, "A review of single phase grid-connected inverters for photovoltaic modules," *IEEE Trans. Ind. Appl.*, vol. 41, no. 5, pp. 1292-1306, Sep.-Oct. 2005.

[3] A. Lohner, T. Meyer, and A. Nagel, "A new panel-integratable inverter concept for grid-connected photovoltaic systems," *Proc. IEEE ISIE'96*, vol. 2, pp. 827-831, 1996.

[4] M. Das and V. Agarwal, "Novel high-performance standalone solar PV system with high-gain high-efficiency DC-DC converter power stages," *IEEE Trans. Ind. Appl.*, vol. 51, no. 6, pp. 4718-4728, Nov. 2015.

[5] C. Jain and B. Singh, "Single-phase single-stage multifunctional grid interfaced solar photo-voltaic system under abnormal grid conditions," *IET Gen, Tran. & Dist.*, vol. 9, no. 10, pp. 886-894, Feb. 2013.

[6] R. K. Agarwal, I. Hussain, B. Singh, "LMF-based control algorithm for single stage three-phase grid integrated solar PV system," *IEEE Trans. Sust. Energy*, vol. 7, no. 4, pp. 1379-1387, Apr. 2016.

[7] C. Jain and B. Singh, "A three-phase grid tied SPV system with adaptive DC link voltage for CPI voltage variations," *IEEE Trans. Sust. Energy*, vol. 7, no. 1, pp. 337-344, Jan. 2016.

[8] S. A. George and F. M. Chacko, "Comparison of different control methods for integrated system of MPPT powered PV module and STATCOM," in *Proc. Int. Conf. Renew. Eenrgy Sustain. Energy*, pp. 207-212, Dec. 5-6, 2013.

[9] S. Kumar, A. K. Verma, I. Hussain, and B. Singh, "Performance of grid interfaced SPV system under variable solar intesity," in *Proc. IEEE 6th India Int. Conf. Power Electron,* pp. 1-6, Dec. 8-10.

[10] B. Singh, D. T. Shahani, and A. K. Verma, "IRPT based ccontrol of a 50kW grid interfaced solar photovoltaic power generating system with power quality improvement," in *Proc. IEEE 4th Int. Symp. Power Electron. Dist. Gen. Syst.*, pp. 1-8, Jul. 8-11.

[11] R. Gupta and A. Ghosh, "Frequency-domain characterization of sliding mode control of an inverter used in DSTATCOM application," *IEEE Trans. Circ. and Syst.*, vol. 53, no. 3, pp. 662-676, 2006.

[12] M. A. Hannnan, Z. Abd Ghani, A. Mohamed, and M. N. Uddin, " Real-time testing of a fuzzy-logic-controller-based grid-connected photovoltaic inverter system," *IEEE TRAns. Ind. Appl.*, vol. 51, no. 6, pp. 4775-4784, Nov-Dec. 2015.

[13] P. Shah, I. Hussain, and B. Singh, "A novel fourth order generalized integrator based control scheme for multifunctional SECS in the distribution system," *IEEE Trans. Energy Conv.*, vol. 33, no. 3, pp. 949-958, Sep. 2018.

[14] D. Yazdani, A. Bakshai, and P. K. Jain, " A three-phase adaptive notch filter-based approach to harmonic/reactive current extraction and harmonic decomposition," *IEEE Trans. Power Electron.*, vol. 25, no. 4, pp. 914-923, 2010.

[15] H. M. Hasanien, "An adaptive control strategy for low voltage ride through capability enhancement of grid-connected photovoltaic power plants," *IEEE Trans. Power Syst.*, vol. 31, no. 4, pp. 3230-3237, Jul. 2016.

[16] Y. Han, M. Luo, X. Zhao, J. M. Guerrero, and L. Xu, "Comparative performance evaluation of orthogonal-signal-generator-based single-phase PLL algorithms - A survey," *IEEE Trans. Power Electron.*, vol. 31, no. 5, pp. 3932-3944, May 2016.

[17] P. Rodriguez, A. Luna, M. Ciobotaru, R. Teodorescu, and F. Blaabjerg, "Advanced grid synchronization system for power converters under unbalanced and distorted operating conditions," in *Proc. 32nd Annu. Conf. IEEE Ind. Electron.*, pp. 5173-5178, Nov. 2006.

[18] M. Ciobotru, R. Teodorescu, and F. Blaabjerg, "A new single-phase PLL structure based on second order generator," in *Proc. 37th IEEE Power Electron. Spec. Conf.*, pp. 1-6, Jun. 2006.

[19] M. Karimi-Ghartemani, S. A. Khajehoddin, P. K. Jain, A. Bakhshai, and M. Mojiri, "Addressing DC component in PLL and notch filter algorithms," *IEEE Trans. Power Electron.*, vol. 27, no. 1, pp. 78-86, Jan. 2012.

[20] S. Golestan, J. M. Guerrero, and J. C. Vasquez, "DC-Offset rejection in phase-locked loops: A novel approach," *IEEE Trans. Ind. Elect.*, vol. 63, no. 8, pp. 4942-4946, Aug. 2016.

[21] J. Matas, H. Martin J. de la Hoz, A. Abusorrah, Y. A. Al-Turki and M. Al-Hindawi, "A family of gradient descent grid frequency estimators for the SOGI filter," *IEEE Trans. Power Elect.*, vol. 33, no. 7, pp. 5796-5810, Jul 2018.

[22] B. Singh, S. Kumar, and C. Jain, "Damped-SOGI-based control algorithm for solar PV power generating system," *IEEE Trans. Ind. Appl.*, vol. 53, no. 3, pp. 1780-1788, May-Jun. 2017.

[23] S. Devassy and B. Singh, "Discrete SOGI based control of solar photovoltaic integrated unified power quality conditioner," *2016 National Power Syst. Conf. (NPSC), Bhubaneswar*, pp. 1-6, 2016.

[24] N. Mohan, T. M. Undeland, and W. P. Robbins, *Power Electronics: Converters Applications and Design.* New York, NY, USA: Wiley, 2003.

[25] J. A. Gow and C. D. Manning, "Development of a photovoltaic array model for use in power-electronics simulation studies," *IET Electr. Power Appl.*, vol. 146, no. 2, pp. 193-200, 1999.
[26] D. Sera, L. Mathe, T. Kerekes, S. V. Spataru, and R. Teodorescu, "On the perturb-and-observe and incremental conductance MPPT methods for PV systems," *IEEE Journ. Photovolt.*, vol. 3, no. 3, pp. 1070-1078, Jul. 2013.
[27] B. Singh, A. Chandra, and K. Al-Haddad, *Power quality: problems and mitigation techniques*, John Wily & Sons, 1^{st} edn. 2014.
[28] Z. Xin, R. Zhao, P. Mattavelli, P. C. Loh, and F. Blaabjerg, "Reinvestigation of generalized integrator based filters from a first-order system perspective," *IEEE Access*, vol. 4, pp. 7131-7144, 2016.
[29] N. Kumar, I. Hussain, B. Singh and B. K. Panigrahi, "Implementation of multilayer fifth-order generalized integrator-based adaptive control for grid-tied solar PV energy conversion system," *IEEE Trans. Indust. Informatics*, vol. 14, no. 7, pp. 2857-2868, Jul. 2018.
[30] Y. F. Wang and Y. W. Li, "Three-phase cascaded delayed signal cancellation PLL for fast selective harmonic detection," *IEEE Trans. Ind. Electron.*, vol. 60, no. 4, pp. 1452-1463, Apr. 2013.
[31] H. Yi, X. Wang, F. Blaabjerg, and F. Zhuo, "Impedance analysis of SOGI-FLL-Based grid synchronization," *IEEE Trans. Power Elect.*, vol. 32, no. 10, pp. 7409-7413, Oct. 2017.

Firdous Ul Nazir received the B.Tech degree in electrical engineering from National Institute of Technology Srinagar, India, in 2012, the M.Tech degree in electrical power systems from Indian Institute of Technology Roorkee, India, in 2015, and the Ph.D. degree from the Department of Electrical and Electronic Engineering, Imperial College London, UK, in 2020. Currently, he is a Research Associate with Imperial College London. His current research interests include distribution system modelling, operation and control, optimization theory, and solar PV to grid integration.

Nishant Kumar (M'15) received the M.Tech. (with Gold Medal) degree in electrical power systems from the National Institute of Technology Durgapur, India, in 2013, and the Ph.D. degree (with Best Thesis Award) in power systems from the Department of Electrical Engineering, IIT Delhi, New Delhi, India, in 2019. He is currently working as a Postdoctoral Research Fellow at National University of Singapore (NUS), Singapore.

From 2013 to 2014, he was the Project Engineer/Research Associate at IIT Bombay and IIT Delhi. His areas of research interests include soft computing-based generation control, optimization algorithm development, and application of soft computing techniques in power system planning, operation, and control.

Bikash C. Pal (M'00-SM'02-F'13) recieved the B.E.E. degree (with honors) from Jadavpur University, Calcutta, India, in 1990, M.E. degree from the Indian Institute of Science, Bangalore, India, in 1992, and the Ph.D. degree from the Imperial College London, London, U.K, in 1999, all in electrical engineering.

Currently, he is a Professor with the Department of Electrical and Electronic Engineering, Imperial College London, London, U.K. His current research interests include state estimation, power system dynamics, and flexible ac transmission system controllers. He was the Editor-in-Chief of the IEEE TRANSACTIONS ON SUSTAINABLE ENERGY (2012-2017) and the Editor-in-Chief of IET Generation, Transmission and Distribution (2005-2012) and is a Fellow of the IEEE for his contribution to power system stability and control. Currently, he is the Vice President Publications of the IEEE Power and Energy Society.

Bhim Singh (SM99, F10) was born in Rahamapur, Bijnor, UP, India, in 1956. He received the B.E. degree in electrical engineering from the University of Roorkee, Roorkee, India, in 1977, and the M.Tech. degree in power apparatus and systems and the Ph.D. degree from Indian Institute of Technology (IIT) Delhi, New Delhi, India, in 1979 and 1983, respectively.

In 1983, he joined the Department of Electrical Engineering, University of Roorkee (now IIT Roorkee), as a Lecturer. He became a Reader there in 1988. In December 1990, he joined the Department of Electrical Engineering, IIT Delhi, as an Assistant Professor, where he has become an Associate Professor in 1994 and a Professor in 1997. He has been the Head in the Department of Electrical Engineering, IIT Delhi, from July 2014 to August 2016. He is currently the Dean, Academics with IIT Delhi. He has guided 70 Ph.D. dissertations, 161 M.E./M.Tech./M.S.(R) thesis. He has executed more than 75 sponsored and consultancy projects.

His areas of research interests include PV grid interface systems, microgrid, power quality, PV water pumping systems, power electronics, electrical machines, drives, FACTS, and HVdc systems.

Bijaya K. Panigrahi (SM'06) received the Ph.D. degree in power system from Sambalpur University, Sambalpur, India, in 2004.

He was a Lecturer with the University College of Engineering, Sambalpur, for 13 years. Since 2005, he has been an Associate Professor in the Department of Electrical Engineering, Indian Institute of Technology (IIT) Delhi, New Delhi, India, where he has become a Professor in 2017.

His research interests include intelligent control of flexible ac transmission system devices, digital signal processing, power quality assessment, and application of soft computing techniques to power system planning, operation and control.